

Article

Characteristics of (002) Oriented Hydroxyapatite Coatings Deposited by Atmospheric Plasma Spraying

Xiaomei Liu ^{1,*} , Dingyong He ^{1,2,*}, Zheng Zhou ^{1,2}, Guohong Wang ², Zengjie Wang ², Xu Wu ² and Zhen Tan ¹

¹ College of Materials Science and Engineering, Beijing University of Technology, Beijing 100124, China; zhouzhengbjut@bjut.edu.cn (Z.Z.); zhen.tan@bjut.edu.cn (Z.T.)

² Beijing Engineering Research Center of Eco-Materials and LCA, Beijing University of Technology, Beijing 100124, China; wanggh@bjut.edu.cn (G.W.); wangzj@bjut.edu.cn (Z.W.); wuxu@bjut.edu.cn (X.W.)

* Correspondence: liuxiaomei@emails.bjut.edu.cn (X.L.); dyhe@bjut.edu.cn (D.H.); Tel.: +86-10-6739-6188 (X.L.)

Received: 16 June 2018; Accepted: 22 July 2018; Published: 25 July 2018



Abstract: Hydroxyapatite (HA) coatings with strong (002) preferred orientation were successfully prepared on Ti-6Al-4V substrates with conventional atmospheric plasma spraying (APS). The intensity changes of (002) preferred orientation along the coating depth were investigated and the mechanical properties of these coatings were analyzed. Results indicated that the intensity of (002) preferred orientation at a distance of longer than ~90 mm from the interface showed a high value, where uniformly distributed columnar grains in a direction perpendicular to the coating surface were observed. The results obtained from experiments on the mechanical properties revealed that the (002) oriented coatings prepared by conventional APS technique exhibited excellent mechanical properties. Meanwhile, this study provided a simple and rapid method for the preparation of HA coatings with (002) preferred orientation.

Keywords: hydroxyapatite coating; atmospheric plasma spraying; preferred orientation; columnar grain

1. Introduction

A high bioactivity and long-term durability hydroxyapatite (HA) coating is required for medical applications. Oriented HA coatings have attracted attention due to their high chemical stabilities and good mechanical properties [1,2]. Research has shown that HA crystals in both long bones and tooth enamel have a preferred orientation [3,4]. Such oriented HA ceramics may enable control over cellular behavior [5,6]. In particular, in vitro behavior has shown that HA crystals with (002) preferred orientation promote cell adhesion [7]. Therefore, the preparation of HA coatings with (002) preferred orientation might be highly reliable in medical applications. The authors have recently found that HA coatings with strong (002) preferred orientation can be obtained on Ti-6Al-4V substrates using a micro-plasma spraying (MPS) process [8–10]. The influence of the spraying parameters on the preferred orientation of MPS-deposited HA coatings was studied. We found that the highest (002) oriented HA coatings were prepared by 60 mm spraying distance with a spraying current of 40 A. At a lower spraying power (<40 A) or shorter spraying distance (<60 mm), the presence of partially melted particles was unfavorable to the formation of preferred orientation. When the spraying current exceeded 40 A, the increased spraying current led to a decrease in the purity and intensity of preferred orientation. At the same spraying current, the dehydroxylation and decomposition of in-flight particles increased and the substrate temperature decreased when the spraying distance increased from 60 to 110 mm, which resulted in weak preferred orientation. Therefore, careful control of the melting

state of in-flight particles and the substrate temperature are required to obtain HA coatings with high (002) preferred orientation. Although the conventional APS technique has been widely used for the fabrication of HA coatings, the preparation and characterization of atmospheric plasma spraying (APS) HA coatings with strong (002) preferred orientation have rarely been previously described [11]. Thus, the aim of the present study was to fabricate HA coatings with (002) preferred orientation by a conventional APS technique according to the relationship between the process parameters and preferred orientation [8–10]. Meanwhile, the microstructure and mechanical properties of the as-sprayed coatings were investigated.

2. Materials and Methods

Commercially spherical hydroxyapatite powders ($\geq 98\%$ purity, Medicoat AG, Mägenwil, Switzerland), with particle sizes of 38–45 μm were used for depositing coatings. Ti-6Al-4V plates ($\Phi 25\text{ mm} \times 3\text{ mm}$) were used as substrates. A conventional APS system with a 9 MB plasma spray gun and 3M7-GH nozzle (SulzerMetco9M, Sulzer Mecto, Pfäffikon, Switzerland) was used to fabricate the HA coatings. The spraying parameters are listed in Table 1. The raw particles were injected vertically into the plasma gun by argon carrier gas. Substrate temperature and coating surface temperature were measured by using an infrared temperature measurement (IMPAC IGA 140, LumaSense Technologies FmbH, Frankfurt, Germany).

Table 1. Plasma spraying parameters.

Current	Voltage	Gas Flow Rate	Spraying Distance	Gun Traverse Speed	Powder Feed Rate	Carrier Gas Flow Rate
330 A	50 V	23 L/min	60 mm	150 m/s	6.5 g/min	5.2 L/min

The as-sprayed and chemically etched cross-section morphologies of HA coatings were observed by Field Emission Scanning Electron Microscopy (FESEM, SU8020, Hitachi, Tokyo, Japan). Coating porosity was estimated using ImageJ 1.49v software. The phase composition of the raw powder and as-sprayed coating was determined by X-ray diffraction (XRD, D8ADVANCE, Bruker AXS GMBH, Bruker, Karlsruhe Germany) using Cu K α radiation [1]. The quantitative analysis of various phases by the Rietveld method has been reported in previous literature [10]. The preferred orientation of the coating was determined with X-ray diffraction (XRD, Rigaku ULTIMA-PC, Rigaku, Tokyo, Japan) using Cu K α radiation. The ratio of (002) to (211) along the coating depth was plotted to analyze the intensity changes of (002) preferred orientation along the coating depth [1].

The bonding strength of the coatings was measured by a universal tensile test machine (CMT5504, SANS Testing Machine Co., Ltd., Shenzhen, China) [12,13]. The specimens were attached to a cylindrical stainless-steel rod using instant adhesive glue (FM1000, Solvay, Brussels, Belgium). The microstructures of the fracture surface were observed by FESEM. Nanoindentation tests were performed using a Nano Indenter System (G200, Agilent, Santa Clara, CA, USA) on the mirror polished cross-sectional surface [14]. Micro-Vickers microhardness tests were performed using a digital microhardness tester (HXD-1000TMC/LCD, Shanghai taiming optical instrument Co. Ltd., Shanghai, China).

3. Results and Discussion

The chemical stability in the body fluid and the mechanical performances of HA coatings must be taken into consideration for medical applications. These performances are influenced not only by the crystallinity, composition, porosity, and surface morphology, but also by the crystallographic texture [15,16]. In this section, the microstructure and mechanical properties of (002) oriented HA coatings were analyzed.

3.1. Microstructure of (002) Oriented HA Coatings

The XRD analysis revealed that the surface layer of the coating consisted of about 85.2% HA, 2.0% tetra-calcium phosphate (TTCP), 3.8% β -tricalcium phosphate (β -TCP), and had a low content CaO phase (\sim 0.7%) (Figure 1a). The weak broad background between about 30° and 35° 2θ of the XRD pattern suggested the formation of minor amorphous calcium phosphate (ACP) (Figure 1a). An ACP content of \sim 8.3% was estimated by the XRD measurements according to the methods by Keller et al. [17]. The content of the HA crystals was \sim 85.2%, which met the $>50\%$ content of HA crystals standard requirements (ISO 13779-2) [18]. The XRD patterns showed that the raw powder exhibited random crystal orientation (Figure 1a). However, the (002) peaks in the as-sprayed coatings appeared more intense and higher than those in the raw powder (Figure 1a), which was evidence of the successful preparation of (002) oriented HA coatings using APS. The ratio of (002) to (211) was plotted to analyze the intensity of the (002) preferred orientation [1], and marked as $I_{(002)}/I_{(211)}$ (Figure 1b). In this work, the $I_{(002)}/I_{(211)}$ was 0.37. The as-sprayed coating exhibited preferred orientation with an $I_{(002)}/I_{(211)}$ of >1.8 . With an increasing distance from the substrate, the intensity of the peak (002) increased. $I_{(002)}/I_{(211)}$ in the upper part ($>90 \mu\text{m}$) exhibited higher values than that in the bottom (Figure 1b). From the polished cross-section of the as-sprayed HA coating, a density structure with a coating thickness of about $180 \mu\text{m}$ was observed (Figure 2a). The porosity was estimated to be approximately 2.7%. The chemically etched morphology of the upper part ($90\text{--}135 \mu\text{m}$) with high $I_{(002)}/I_{(211)}$ values corresponded to a lamellar structure with uniformly distributed columnar grains in a direction perpendicular to the coating, and the growth of columnar grains did not go beyond the splat-splat boundary (Figure 2b(4)). However, a columnar structure was not obviously observed from the bottom of the coating (Figure 2b(1)) and the intensity of the (002) orientation in this region was weak (Figure 1b).

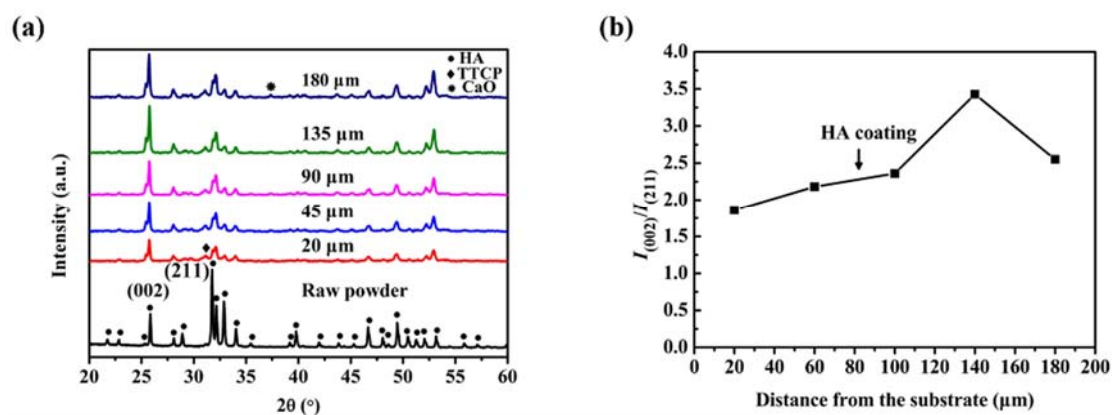


Figure 1. (a) XRD patterns of raw powder and XRD patterns at different distances from the coating/substrate interface in the as-sprayed HA coating, and (b) (002) orientation intensity variations along the coating depth.

In this study, the surface temperature of the in-flight particles within a range of $1749.9\text{--}2321.8^\circ\text{C}$ was above the melting point of HA (1550°C). The velocity of the in-flight particles was in the range of $159.5\text{--}168.9 \text{ m/s}$. The low velocities observed in this work were attributed to a low argon flow rate and low spraying current. In this case, the long dwell time of the in-flight particles in the plasma jet was sufficient to melt all of the in-flight particles before deposition. Therefore, the in-flight particles with a fully melted state struck the substrate, deformed, and solidified to form a lamellar structure. The microstructure of the deposited lamella depends on the cooling rate of the particles during solidification [19]. The fully melted in-flight particles impacting the substrate with an initial temperature of 25°C led to large temperature difference between the droplet and substrate. As we know, the large temperature difference and high thermal conductivity of the metal substrate accelerate

the rate of heat removal at the coating–substrate interface, leading to high cooling rate. The high cooling rate in this region promotes the formation of ACP [20] and restricts the formation of columnar grains. Consequently, no obvious columnar grains were observed from the bottom of the coating (Figure 2b(1)), which corresponded to weak preferred orientation (Figure 1). Once a layer has been deposited on the whole substrate, the gun returns to the initial position and the second layer is coated. A short spraying distance of 60 mm and low gun traverse speed of 150 m/s were used to make the substrate experience more of the heating effects of the plasma flame. Under the experimental conditions, the heat accumulation from the plasma flame, the incoming droplets, and the latent heat from the crystallization increased the local temperature to ~ 450 °C. Moreover, the subsequent particles struck onto the previously deposited coating. Thus, the thermal conductivity of the underlying materials decreased [21]. These factors led to the decrease of the lamella cooling rate. Under such conditions, the columnar grains had enough time to grow along the direction of the heat flux which was perpendicular to the substrate surface. When the third layer was coated, the local temperature of the prior-formed coating reached up to 510 °C. The high local temperature contributed to the growth of columnar grains. Therefore, uniformly distributed columnar grains could be formed in the upper part of coating (90–180 μm).

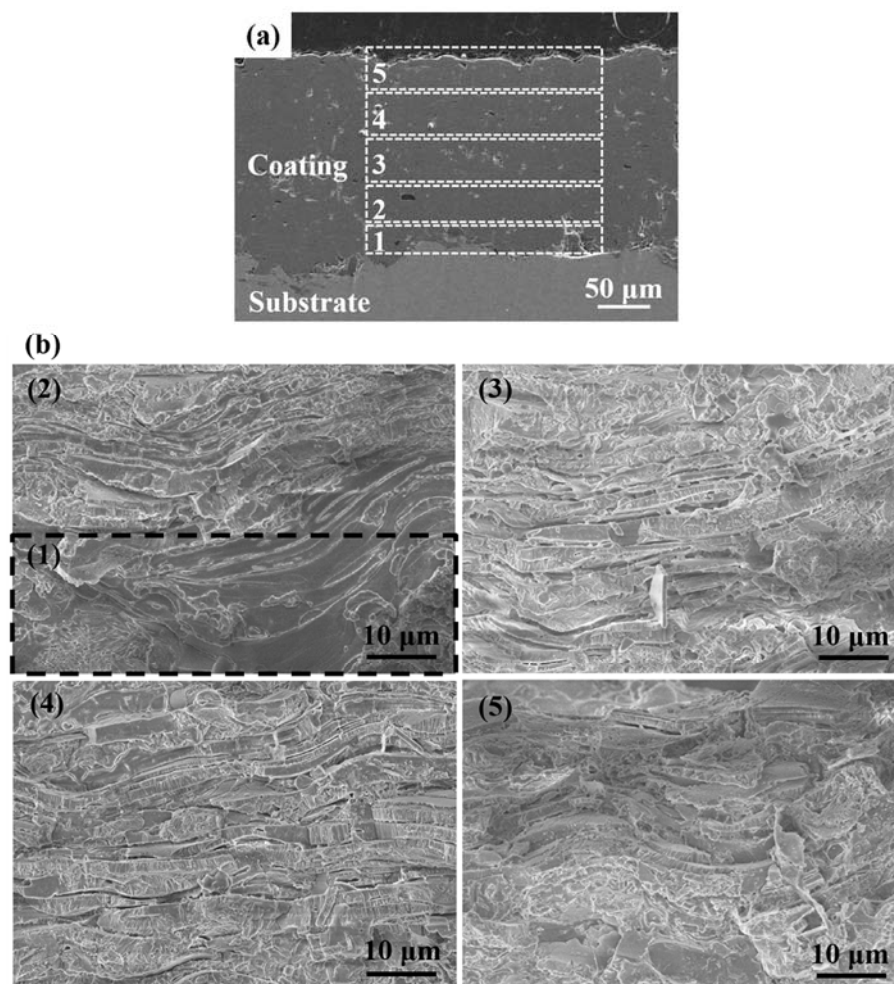


Figure 2. (a) Cross-section morphology of the as-sprayed HA coating, and (b) SEM morphologies of the chemically etched cross-section of the as-sprayed HA coating.

3.2. Mechanical Properties of (002) Oriented Coatings

Bond strength is an important property of HA coatings. The tensile test revealed the bonding strength of the HA coating with a strong (002) preferred orientation up to 19.1 ± 1.5 MPa. Fracture surface analysis suggested that the failure modes of those coatings involved both cohesion failure and adhesion failure (Figure 3a). The magnified image of the fracture surface is shown in Figure 3c. There was clear evidence that the internal fracture of a single splat occurred. Columnar grains were also observed, which showed that the existence of columnar grains could prevent crack propagation.

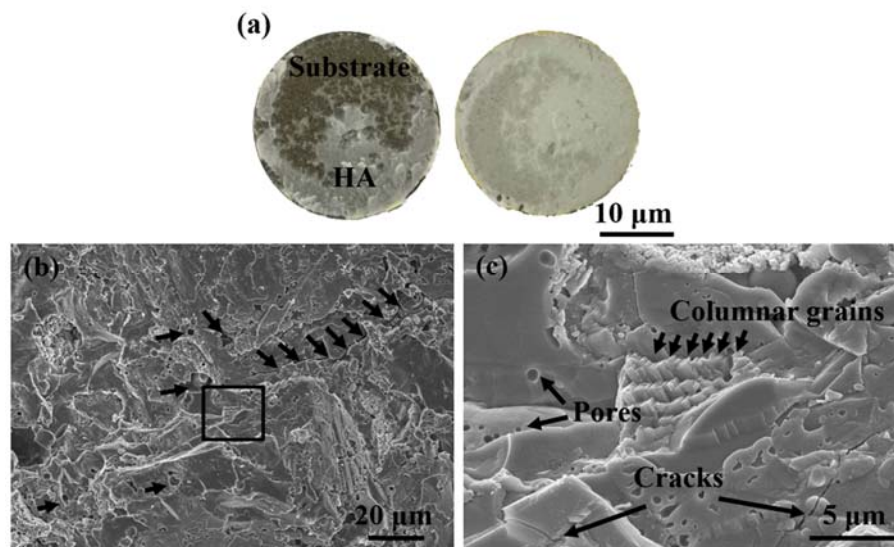


Figure 3. (a) Photographs after bonding strength test; (b) SEM image of fracture surface; (c) SEM image of fracture surface at high magnification.

Hardness and elastic modulus are important parameters for biological coatings on the surface of implants. Nanoindentation was used to measure the hardness and elastic modulus of the (002) oriented coatings. Figure 4 shows the hardness-depth (Figure 4a) and elastic modulus-depth curves (Figure 4b) of the (002) oriented coatings at different positions. The average hardness of the coating was found to be 4.7 ± 0.5 GPa and the average elastic modulus was 83.3 ± 7.5 GPa.

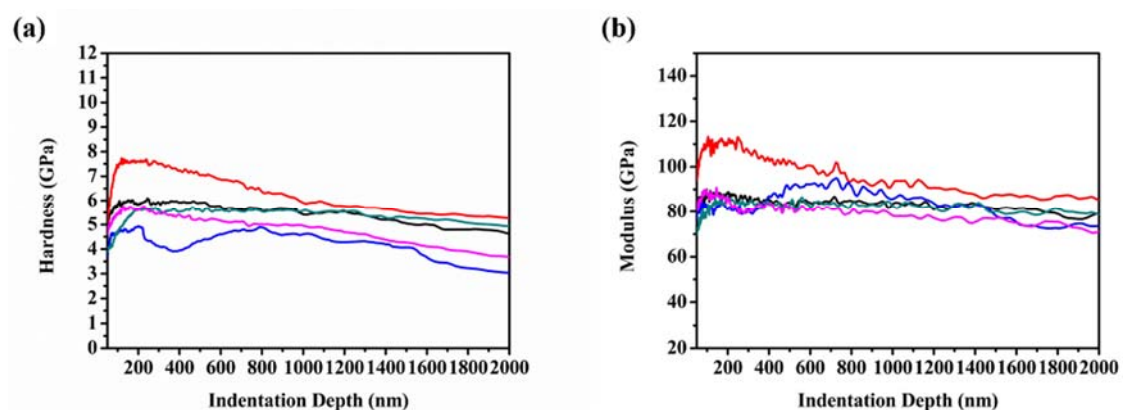


Figure 4. (a) hardness-depth curves of (002) oriented coatings at different positions, and (b) elastic modulus-depth curves of (002) oriented coatings at different positions. In this figure, the different colors represent different positions. Hardness and elastic modulus were measured at different positions of HA coatings to get average value.

The fracture toughness of the coatings was calculated as follows [22,23]:

$$K_{IC} = 0.016(E/H)^{(1/2)} (P/C)^{(3/2)} \quad (1)$$

where E is the elastic modulus of the coating; H is the hardness of the coating; P is the indenter load; and C is the crack length caused by indentation. After calculation, the fracture toughness values of $1.7 \pm 0.2 \text{ MPa m}^{1/2}$ were estimated for the (002) oriented coatings. Compared with other studies for conventional HA coatings fabricated using plasma spraying [24], the (002) oriented coatings revealed a higher hardness, elastic modulus, and fracture toughness. The experimental results demonstrated that (002) oriented coatings prepared by conventional APS technique could improve the mechanical properties of implants. In addition, further studies are needed to elucidate the osteoconductivity of these coatings.

4. Conclusions

Hydroxyapatite (HA) coatings with strong (002) preferred orientation were successfully prepared on Ti-6Al-4V substrates by a conventional APS technique. The intensity changes of preferred orientation along the coating depth were investigated. The results indicated that the intensity of the (002) orientation in the upper part of the HA coating (90–180 μm) exhibited higher values than that at the bottom. The morphology of this region corresponded to a lamellar structure with uniformly distributed columnar grains in a direction perpendicular to the coating surface. The experimental results indicate that the (002) oriented HA coatings prepared by a conventional APS technique exhibited good mechanical properties.

Author Contributions: Conceptualization, X.L., D.H., and Z.Z.; Methodology, X.L.; Formal Analysis, X.L., D.H., Z.Z., G.W., Z.W., X.W., and Z.T.; Writing-Original Draft Preparation, X.L.; Writing-Review & Editing, X.L., and D.H.

Funding: This research was funded by the National Natural Science Foundation of China (51471010).

Acknowledgments: The authors would like to gratefully thank F. Yang, College of Foreign Languages, Beijing University of Technology, for her kind assistance with the English writing.

Conflicts of Interest: The authors declare no conflict of interest.

References

1. Wang, Y.; Liu, X.; Fan, T.; Tan, Z.; Zhou, Z.; He, D. In vitro evaluation of hydroxyapatite coatings with (002) crystallographic texture deposited by micro-plasma spraying. *Mater. Sci. Eng. C* **2017**, *75*, 596–601. [[CrossRef](#)] [[PubMed](#)]
2. Kim, H.; Camata, R.P.; Chowdhury, S.; Vohra, Y.K. In vitro dissolution and mechanical behavior of c -axis preferentially oriented hydroxyapatite thin films fabricated by pulsed laser deposition. *Acta Biomater.* **2010**, *6*, 3234–3241. [[CrossRef](#)] [[PubMed](#)]
3. Wenk, H.R.; Heidelbach, F. Crystal alignment of carbonated apatite in bone and calcified tendon: Results from quantitative texture analysis. *Bone* **1999**, *24*, 361–369. [[CrossRef](#)]
4. Fujisaki, K.; Todoh, M.; Niida, A.; Shibuya, R.; Kitami, S.; Tadano, S. Orientation and deformation of mineral crystals in tooth surfaces. *J. Mech. Behav. Biomed.* **2012**, *10*, 176–182. [[CrossRef](#)] [[PubMed](#)]
5. Almora-Barrios, N.; Austen, K.F.; de Leeuw, N.H. Density functional theory study of the binding of glycine, proline, and hydroxyproline to the hydroxyapatite (0001) and (0110) surfaces. *Langmuir* **2009**, *25*, 5018–5025. [[CrossRef](#)] [[PubMed](#)]
6. Dong, X.; Zhou, H.; Wu, T.; Wang, Q. Behavior regulation of adsorbed proteins via hydroxyapatite surface texture control. *J. Phys. Chem. C* **2008**, *112*, 4751–4759. [[CrossRef](#)] [[PubMed](#)]
7. Kim, H.; Camata, R.P.; Lee, S.; Rohrer, G.S.; Rollett, A.D.; Hennessy, K.M.; Vohra, Y.K. Calcium phosphate bioceramics with tailored crystallographic texture for controlling cell adhesion. *Mater. Res. Soc. Symp. Proc.* **2006**, *925*, 0925-BB02-07. [[CrossRef](#)]
8. Wang, Y.; Fan, T.; Zhou, Z.; He, D. Hydroxyapatite coating with strong (002) crystallographic texture deposited by micro-plasma spraying. *Mater. Lett.* **2016**, *185*, 484–487. [[CrossRef](#)]

9. Liu, X.; He, D.; Wang, Y.; Zhou, Z.; Wang, G.; Tan, Z.; Wang, Z. The influence of spray parameters on the characteristics of hydroxyapatite in-flight particles, splats and coatings by micro-plasma spraying. *J. Therm. Spray Technol.* **2018**, *27*, 667–679. [[CrossRef](#)]
10. Liu, X.; He, D.; Zhou, Z.; Wang, Z.; Wang, G. The influence of process parameters on the structure, phase composition, and texture of micro-plasma sprayed hydroxyapatite coatings. *Coatings* **2018**, *8*, 106. [[CrossRef](#)]
11. Tong, W.; Chen, J.; Li, X.; Feng, J.; Cao, Y.; Yang, Z.; Zhang, X. Preferred orientation of plasma sprayed hydroxyapatite coatings. *J. Mater. Sci.* **1996**, *31*, 3739–3742. [[CrossRef](#)]
12. Li, H.; Khor, K.A.; Cheang, P. Adhesive and bending failure of thermal sprayed hydroxyapatite coatings: Effect of nanostructures at interface and crack propagation phenomenon during bending. *Eng. Fract. Mech.* **2007**, *74*, 1894–1903. [[CrossRef](#)]
13. Kweh, S.W.; Khor, K.A.; Cheang, P. Plasma-sprayed hydroxyapatite (HA) coatings with flame-spheroidized feedstock: Microstructure and mechanical properties. *Biomaterials* **2000**, *21*, 1223–1234. [[CrossRef](#)]
14. Liu, X.; Song, X.; Wang, H.; Hou, C.; Liu, X.; Wang, X. Reinforcement of tungsten carbide grains by nanoprecipitates in cemented carbides. *Nanotechnology* **2016**, *27*, 415710. [[CrossRef](#)] [[PubMed](#)]
15. Filgueiras, M.R.T.; Mkhonto, D.; de Leeuw, N.H. Computer simulations of the adsorption of citric acid at hydroxyapatite surfaces. *J. Cryst. Growth* **2006**, *294*, 60–68. [[CrossRef](#)]
16. Chen, W.; Tian, B.; Lei, Y.; Ke, Q.; Zhu, Z.; Guo, Y. Hydroxyapatite coatings with oriented nanoplate and nanorod arrays: Fabrication, morphology, cytocompatibility and osteogenic differentiation. *Mater. Sci. Eng. C* **2016**, *67*, 395–408. [[CrossRef](#)] [[PubMed](#)]
17. Keller, L.; Dollase, W.A. X-ray determination of crystalline hydroxyapatite to amorphous calcium-phosphate ratio in plasma sprayed coatings. *J. Biomed. Mater. Res.* **2003**, *49*, 244–249. [[CrossRef](#)]
18. *ISO 13779-2 Implants for Surgery-Hydroxyapatite. Part 2: Coatings of Hydroxyapatite*; International Organization for Standardization: Geneva, Switzerland, 2008.
19. Moreau, C.; Lamontagne, M.; Cielo, P. Influence of the coating thickness on the cooling rates of plasma-sprayed particles impinging on a substrate. *Surf. Coat. Technol.* **1992**, *53*, 107–114. [[CrossRef](#)]
20. Gross, K.A.; Berndt, C.C.; Herman, H. Amorphous phase formation in plasma-sprayed hydroxyapatite coatings. *J. Biomed. Mater. Res.* **1998**, *39*, 407–414. [[CrossRef](#)]
21. Wen, J.; Yang, L.; Chen, J.; Zhang, C. Chemical gradient in plasma-sprayed HA coatings. *Biomaterials* **2000**, *21*, 1339–1343. [[CrossRef](#)]
22. Liu, Y.; Dang, Z.; Wang, Y.; Huang, J.; Li, H. Hydroxyapatite/graphene-nanosheet composite coatings deposited by vacuum cold spraying for biomedical applications: Inherited nanostructures and enhanced properties. *Carbon* **2014**, *67*, 250–259. [[CrossRef](#)]
23. Li, H.; Khor, K.A.; Cheang, P. Young's modulus and fracture toughness determination of high velocity oxy-fuel-sprayed bioceramic coatings. *Surf. Coat. Technol.* **2002**, *155*, 21–32. [[CrossRef](#)]
24. Dey, A.; Mukhopadhyay, A.K.; Gangadharan, S.; Sinha, M.K.; Basu, D.; Bandyopadhyay, N.R. Nanoindentation study of microplasma sprayed hydroxyapatite coating. *Ceram. Int.* **2009**, *35*, 2295–2304. [[CrossRef](#)]

